Physica Scripta. Vol. 71, 280–292, 2005

Small-angle Scattering Theory Revisited: Photocurrent and Spatial Localization

N. P. Basse*[1], S. Zoletnik[2] and P. K. Michelsen[3]

[1]Plasma Science and Fusion Center, Massachusetts Institute of Technology, MA-02139 Cambridge, USA
[2]CAT-Science Bt., Detrekő u. 1/b, H-1022 Budapest, Hungary and Association EURATOM – KFKI-RMKI, H-1125 Budapest, Hungary
[3]Association EURATOM – Risø National Laboratory, DK-4000 Roskilde, Denmark

Received June 4, 2004; accepted July 27, 2004

PACS numbers: 52.25.Gj, 52.25.Rv, 52.35.Ra, 52.55.Hc, 52.70.Kz

Abstract

In this paper theory on collective scattering measurements of electron density fluctuations in fusion plasmas is revisited. We present the first full derivation of the expression for the photocurrent beginning at the basic scattering concepts. Thereafter we derive detailed expressions for the auto- and crosspower spectra obtained from measurements. These are discussed and simple simulations made to elucidate the physical meaning of the findings. In this context, the known methods of obtaining spatial localization are discussed and appraised. Where actual numbers are applied, we utilize quantities from two collective scattering instruments: The ALTAIR diagnostic on the Tore Supra tokamak [A. Truc *et al*., "ALTAIR: An infrared laser scattering diagnostic on the Tore Supra tokamak," Rev. Sci. Instrum. **63**, 3716–3724 (1992)]. and the LOTUS diagnostic on the Wendelstein 7-AS stellarator [M. Saffman *et al*., "CO_2 laser based two-volume collective scattering instrument for spatially localized turbulence measurements," Rev. Sci. Instrum. **72**, 2579–2592 (2001)].

I. Introduction

A. Motivation

In this paper we will revisit theoretical aspects of small-angle collective scattering of infrared light off electron density fluctuations. Our main reasons for this second look are the following:

- Working through the literature, we have found that most of the information needed for a full treatment of scattering is indeed available, but distributed among numerous authors. Further, some of these sources are not readily available. We here collect those results and present one coherent derivation from basic scattering concepts to the analytical expression for the detected photocurrent.
- It has been important to us to present *understandable* derivations throughout the paper. In most cases all steps are included, removing the necessity to make separate notes. One exception is section III A 2.
- The theory is reviewed from a practical point of view; the work done is in support of measurements of density fluctuations in the Wendelstein 7-AS (W7-AS) stellarator [1]. Here, we used a CO_2 laser having a wavelength of 10.59 μm to make small-angle measurements [2–8].
- A number of points have been clarified, for instance the somewhat confusing term 'antenna' or 'virtual local oscillator' beam. Further, several minor corrections to the derivations in previous work have been included.
- Spatial localization of the density fluctuations measured using collective scattering is of central importance [9]. We review the methods available and discuss the pros and cons of these techniques.

The paper constitutes a synthesis between collective light scattering theory and experiment which will be useful for theoreticians and experimentalists alike in interpreting measurements.

As we have noted, the sources of information on the theory of collective scattering are spread over several decades and authors. We will make it clear in the paper where we use them.

B. Collective scattering measurements

In 1960 the first laser was demonstrated [10], which provided a stable source of monochromatic radiation.

The first observation of density fluctuations in a fusion device using laser scattering was made by C. M. Surko and R. E. Slusher in the Adiabatic Toroidal Compressor (ATC) tokamak [11].

Subsequently, detection of density fluctuations using lasers has been performed in numerous machines, both applying the technique used in the ATC tokamak [12–17] and related methods, e.g. far-infrared (FIR) scattering [18–20] and phase-contrast imaging (PCI) [21–23].

Scattering using infrared light has several advantages over alternative systems: The technique is non-intrusive, i.e. it does not perturb the investigated plasma in any way. Refraction effects can be neglected due to the high frequency of the laser radiation. Further, fluctuations can be measured at all densities, the lower density limit only depending on the signal-to-noise ratio (SNR) of the acquisition electronics.

The major drawback of collective scattering is spatial localization: Direct localization, where the measurement volume is limited in size by crossing beams is only possible for extremely large wavenumbers where the fluctuation amplitude is known to be minute. However, several methods of indirect localization have been developed; one where two measurement volumes overlap in the plasma [24], one where the change of the magnetic field direction along the measurement volume is taken into account [16] and a third design which is an updated version of the crossed beam technique [2].

Summarizing the state of collective scattering diagnostics on fusion machines in 2005: A large amount of measurements has been made in these devices. The massive database strongly suggests that the density fluctuations created by turbulence cause strong transport of energy and particles out of the plasma. However, a consistent detailed picture of how the various turbulent components are correlated with global transport has not yet emerged.

C. Organization of the paper

The paper is organized as follows: In section II, we derive an expression for the detected photocurrent from first principles.

*Electronic address: basse@psfc.mit.edu; URL: http://www.psfc.mit.edu/people/basse/

Thereafter demodulation is explained, phase separation of the detected signal is interpreted and an expression for the density fluctuations squared is presented. Finally, a simple example illustrates this density fluctuation formula for Gaussian beams. In section III, the measurement volume is treated in detail. The simple geometrical estimate is compared to a more elaborate treatment. Following this, direct and indirect localization is discussed, and general expressions for auto- and crosspower are derived. A discussion ensues, and finally simulations assist in the interpretation of localized autopower from a single measurement volume. Section IV states our main conclusions.

II. Collective Light Scattering

In this section we will investigate the theoretical aspects of scattering in detail. The main result will be the derivation of an expression for the observed photocurrent (section II D, Eq. (29)).

A classification of scattering is found in section II A, and the scattering cross section is briefly reviewed in section II B. Basic scattering theory is described in section II C, and a derivation of the detected photocurrent is the subject of section II D. Retrieval of the complex signal using demodulation is explained in section II E. The relationship between the observed phase and the direction of motion is explored in section II F. The final section (II G) deals with spectral theory applied to the derived photocurrent.

A. Scattering classification

We would like to touch upon a few subjects relating to the type of scattering that is observed. First of all a classification of scattering is useful [25]:

- If one were to describe scattering of an electromagnetic field off a particle quantum mechanically, the description would be of photons bouncing off the particle.
  1. Thomson scattering: Negligible change in mean particle momentum during collision with the photon ($\hbar\omega \ll mc^2$).
  2. Compton scattering: The case where photons are so energetic that their momentum cannot be ignored.

  As we work with a wavelength $\lambda_0 = 10.59\,\mu\text{m}$ in the infrared range, the photon energy is much smaller than the rest mass of the electron. Therefore we will restrict ourselves to consider classical Thomson scattering.
- Since the ions are much heavier than the electrons, their acceleration and hence radiation is usually sufficiently small to be ignored. So the electrons do the scattering.
- The Salpeter parameter $\alpha_S = 1/k\lambda_D$ [26] determines whether the scattering observed is incoherent ($\alpha_S < 1$) or coherent ($\alpha_S > 1$). Here, k is the wavenumber observed and $\lambda_D = \sqrt{\varepsilon_0 T/ne^2}$ is the Debye length. Basically, incoherent scattering is due to scattering off single electrons, while coherent scattering is due to scattering off a bunch of electrons; this is also known as collective scattering and is the limit we are observing with the W7-AS diagnostic.

To sum up, we are dealing with collective Thomson scattering. Four elements go into the process of scattering:

1. The incident radiation (the laser beam).
2. The set of scatterers (electrons).
3. The reference beam.
4. The detector.

In this paper we describe the first 3 parts; a description of the detectors used is to be found in Ref. 2 which also contains a detailed description of the practical implementation of the localized turbulence scattering (LOTUS) diagnostic.

B. Scattering cross section

The power P per unit solid angle Ω_s scattered at an angle ζ by an electron is given by

$$\frac{\mathrm{d}P}{\mathrm{d}\Omega_s} = \sqrt{\frac{\varepsilon_0}{\mu_0}}|\mathcal{E}_0^2| r_e^2 \sin^2\zeta, \tag{1}$$

where $\sqrt{\frac{\varepsilon_0}{\mu_0}}|\mathcal{E}_0^2|$ (see section II C 1 for the definition of $\mathcal{E}_0$) is the incident laser power per unit area,

$$r_e = \frac{\mu_0 e^2}{4\pi m_e} \tag{2}$$

is the classical electron radius and ζ is the angle between the incident and scattered power [25]. The scattering cross section σ per unit solid angle is then defined as

$$\frac{\mathrm{d}\sigma}{\mathrm{d}\Omega_s} = \frac{\mathrm{d}P}{\mathrm{d}\Omega_s}\frac{1}{\sqrt{\frac{\varepsilon_0}{\mu_0}}|\mathcal{E}_0^2|} = r_e^2 \sin^2\zeta \tag{3}$$

Knowing that $\mathrm{d}\Omega_s = 2\pi \sin\zeta\,\mathrm{d}\zeta$ we get

$$\sigma = \int \mathrm{d}\sigma = 2\pi r_e^2 \int_0^\pi \sin^3\zeta\,\mathrm{d}\zeta = 2\pi r_e^2 (4/3), \tag{4}$$

which one could interpret as an effective size of the electron for scattering.

We now wish to rewrite the classical electron radius using the polarizability α, defined by the equation for the dipole moment $\mathbf{p}$

$$\mathbf{p} = \alpha\varepsilon_0 \mathbf{E}, \tag{5}$$

where $\mathbf{E}$ is the incident electric field [27]. If this electric field possesses a harmonic time variation with frequency ω, the electron will execute an undamped, forced oscillation [28]. The equation of motion can be solved for the electron position, leading to a determination of the dipole moment. Using Eq. (5) we then calculate the static ($\omega = 0$) polarizability α_0

$$\alpha_0 = \frac{e^2}{\varepsilon_0 m_e \omega_0^2} = \frac{\mu_0 e^2}{m_e}\frac{c^2}{\omega_0^2} = \frac{\mu_0 e^2}{m_e}\frac{1}{k_0^2}, \tag{6}$$

where $\omega_0 = ck_0$ is the eigenfrequency of the electron [27]. Eq. (6) enables us to express the classical electron radius in terms of α_0

$$r_e = \frac{k_0^2 \alpha_0}{4\pi} \tag{7}$$

C. Scattering theory

1. Radiation source. Our incident laser beam has a direction $\mathbf{k}_0$, where $k_0 = \omega_0/c$, and a wavelength $\lambda_0 = 10.59\,\mu\text{m}$. For a linearly polarized beam, the electric field is given as in Eq. (8), where $\mathcal{E}_0(\mathbf{r}) = \mathcal{E}_0 u_0(\mathbf{r}) e^{\mathrm{i}(\mathbf{k}_0 \cdot \mathbf{r})}$ [29]. $\mathcal{E}_0$ is a vector whose direction and amplitude are those of the electric field at maximum.

$$\mathbf{E}_0(\mathbf{r}, t) = Re\{\mathcal{E}_0(\mathbf{r}) e^{-\mathrm{i}\omega_0 t}\} \tag{8}$$

Assuming Gaussian beams, the radial profile near the waist w will be of the form $u_0(\mathbf{r}) = e^{-(r_\perp^2/w^2)}$, where $r_\perp$ is the perpendicular distance from the beam axis.

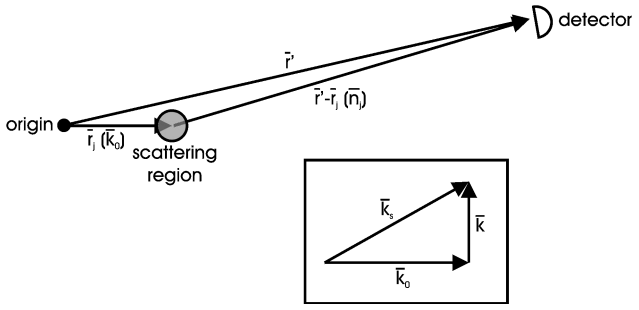

Fig. 1. Scattering geometry. Main figure: The position of a scatterer is $\mathbf{r}_j$ and $\mathbf{r}'$ is the detector position. Inset: The incoming wave vector $\mathbf{k}_0$ and scattered wave vector $\mathbf{k}_s$ determine the observed wave vector $\mathbf{k}$.

The frequency of the laser radiation ω_0 is much higher than the plasma frequency $\omega_\mathrm{p} = \sqrt{ne^2/\varepsilon_0 m_\mathrm{e}}$. This means that the refractive index of the plasma

$$N = \sqrt{1 - \omega_\mathrm{p}^2/\omega_0^2} \tag{9}$$

is close to one, or that refractive effects are negligible [30]. This is a significant advantage compared to microwave diagnostics, where raytracing calculations must assist interpretation of the measurements.

2. Single particle scattering. For a single scatterer having index j located at position $\mathbf{r}_j$ (see Fig. 1), the scatterer radiates an electric field at $\mathbf{r}'$ (the detector position) as a result of the incident beam field. This field is given in Eq. (10), where $\mathbf{n}_j$ is along $\mathbf{r}' - \mathbf{r}_j$ and approximately perpendicular to $\mathcal{E}_0$ [31]

$$\mathbf{E}_s(\mathbf{r}', t) = Re\{\mathcal{E}_s(\mathbf{r}')e^{-\mathrm{i}\omega_0 t}\}$$
$$\mathcal{E}_s(\mathbf{r}') = \left\{ \frac{k_0^2\alpha_0}{4\pi} \frac{e^{\mathrm{i}k_0|\mathbf{r}'-\mathbf{r}_j|}}{|\mathbf{r}' - \mathbf{r}_j|}[\mathbf{n}_j \times \mathcal{E}_0(\mathbf{r}_j)] \times \mathbf{n}_j \right\} \tag{10}$$

The scattered field is simply the radiation field from an oscillating dipole having a moment $\mathbf{p}$ [32]

$$\mathbf{E} = \frac{k^2}{4\pi\varepsilon_0} \frac{e^{\mathrm{i}kr}}{r}[\mathbf{n} \times \mathbf{p}] \times \mathbf{n} \tag{11}$$

Therefore the above expression for the scattered electric field is often called the dipole approximation. It is an approximation because the equation is only valid in the nonrelativistic limit. For very energetic electrons the relativistic corrections become significant, see e.g. Ref. 25.

3. Far field approximation. Two assumptions are made:

1. The position where one measures ($\mathbf{r}'$) is far from the scattering region.
2. The opening angle of the detector is small,

leading to the validity of the far field approximation [31]. This means that we can consider the scattered field from all j particles in the scattering volume to have the same direction denoted $\mathbf{n}'$ parallel to $\mathbf{n}_j$. Therefore the scattered wave vector $\mathbf{k}_s = k_0\mathbf{n}'$ and $\mathbf{k} = \mathbf{k}_s - \mathbf{k}_0$ is the wave vector selected by the optics, see Fig. 1.

The scattered field at the detector due to several particles can be written as a sum [31]

$$\mathbf{E}_s(\mathbf{r}', t) = Re\{\mathcal{E}_s(\mathbf{r}')e^{-\mathrm{i}\omega_0 t}\}$$
$$\mathcal{E}_s(\mathbf{r}') = \frac{k_0^2\alpha_0}{4\pi} \sum_j \frac{e^{\mathrm{i}k_0|\mathbf{r}'-\mathbf{r}_j|}}{|\mathbf{r}' - \mathbf{r}_j|} u_0(\mathbf{r}_j)[\mathbf{n}' \times \mathcal{E}_0] \times \mathbf{n}' e^{\mathrm{i}\mathbf{k}_0\cdot\mathbf{r}_j} \tag{12}$$

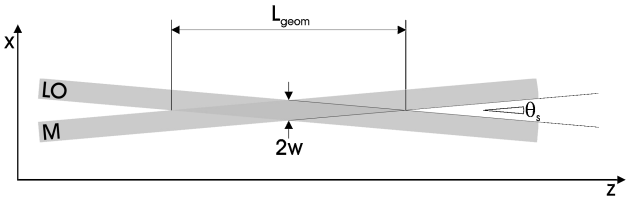

Fig. 2. Scattering geometry. The main (M) and local oscillator (LO) beams cross at an angle thereby creating an interference pattern.

In going from a single particle scattering description to more particles, we will approximate the position of the individual scatterers $\mathbf{r}_j$ by one common vector $\mathbf{r}$. The particles will have a density distribution $n(\mathbf{r}, t)$. We write the scattered field as an integral over the measurement volume V

$$\mathcal{E}_s(\mathbf{r}', t) = \frac{k_0^2\alpha_0}{4\pi} \int_V \frac{e^{\mathrm{i}k_0|\mathbf{r}'-\mathbf{r}|}}{|\mathbf{r}' - \mathbf{r}|} u_0(\mathbf{r})[\mathbf{n}' \times \mathcal{E}_0] \times \mathbf{n}' n(\mathbf{r}, t) e^{\mathrm{i}\mathbf{k}_0\cdot\mathbf{r}} \mathrm{d}^3\mathbf{r} \tag{13}$$

D. The photocurrent

The electric field of the local oscillator (LO, see Fig. 2) beam along $\mathbf{n}'$ at the detector is given as

$$\mathbf{E}_\mathrm{LO}(\mathbf{r}', t) = Re\{\mathcal{E}_\mathrm{LO}(\mathbf{r}')e^{-\mathrm{i}(\omega_0+\omega_\Delta)t}\}$$
$$\mathcal{E}_\mathrm{LO}(\mathbf{r}') = \mathcal{E}_\mathrm{LO} u_\mathrm{LO}(\mathbf{r}')e^{\mathrm{i}k_0\mathbf{n}'\cdot\mathbf{r}'}, \tag{14}$$

where ω_Δ is a frequency shift and $\mathbf{k}_\mathrm{LO} = \mathbf{k}_s = k_0\mathbf{n}'$ [29].

The incident optical power reaching the detector can be found integrating the Poynting vector over the detector area A [29]

$$\begin{aligned} S(t) &= \frac{1}{\mu_0} \int_A (\mathbf{E} \times \mathbf{B}) \cdot \mathrm{d}^2\mathbf{r}' \\ &= \frac{1}{\mu_0 c} \int_A |\mathbf{E}_\mathrm{LO}(\mathbf{r}', t) + \mathbf{E}_s(\mathbf{r}', t)|^2 \mathrm{d}^2\mathbf{r}' \\ &= \frac{1}{\mu_0 c} \int_A |\mathbf{E}_\mathrm{LO}(\mathbf{r}', t)|^2 + |\mathbf{E}_s(\mathbf{r}', t)|^2 + 2 \\ &\quad \times Re\{\mathbf{E}_\mathrm{LO}^*(\mathbf{r}', t)\mathbf{E}_s(\mathbf{r}', t)\} \mathrm{d}^2\mathbf{r}' \end{aligned} \tag{15}$$

What we are interested in is the last term of the equation, namely the beating term

$$S_\mathrm{B}(t) = \int_A \frac{2}{\mu_0 c} Re\{\mathbf{E}_\mathrm{LO}^*(\mathbf{r}', t)\mathbf{E}_s(\mathbf{r}', t)\} \mathrm{d}^2\mathbf{r}' \tag{16}$$

The term containing the LO power is constant, and the contribution to the power from the scattered field is very small because its field amplitude is much smaller than that of the LO [31].

Now we define the integrand of Eq. (16) to be $s_\mathrm{B}(\mathbf{r}')$

$$\begin{aligned} s_\mathrm{B}(\mathbf{r}') &= \frac{2}{\mu_0 c} Re\{\mathbf{E}_\mathrm{LO}^*(\mathbf{r}', t)\mathbf{E}_s(\mathbf{r}', t)\} \\ &= 2\sqrt{\frac{\varepsilon_0}{\mu_0}} Re\{\mathcal{E}_s(\mathbf{r}') \cdot \mathcal{E}_\mathrm{LO}^*(\mathbf{r}')e^{\mathrm{i}\omega_\Delta t}\} \end{aligned} \tag{17}$$

Assuming a detector quantum efficiency η leads to the photocurrent [29]

$$i_\mathrm{B}(t) = \frac{e\eta}{\hbar\omega_0} \int_A s_\mathrm{B}(\mathbf{r}') \mathrm{d}^2\mathbf{r}' \tag{18}$$

The photocurrent due to an ensemble of scatterers at the detector position $\mathbf{r}'$ (replacing i_B by i_k, where the subscript k is

the measured wavenumber) is

$$i_k(t)\frac{\hbar\omega_0}{e\eta} = \int_A s_B(\mathbf{r}')d^2\mathbf{r}' = 2Re\left\{\frac{1}{\mu_0 c}\int_A [\mathbf{E}^*_{LO}(\mathbf{r}',t)\mathbf{E}_s(\mathbf{r}',t)]d^2\mathbf{r}'\right\}$$
$$= 2Re\left\{\frac{1}{\mu_0 c}\int_A\left[\mathcal{E}^*_{LO}u^*_{LO}(\mathbf{r}')e^{-ik_0\mathbf{n}'\cdot\mathbf{r}'}e^{it(\omega_0+\omega_\Delta)}\right.\right.$$
$$\times\frac{k_0^2\alpha_0}{4\pi}\int_V\frac{e^{ik_0|\mathbf{r}'-\mathbf{r}|}}{|\mathbf{r}'-\mathbf{r}|}u_0(\mathbf{r})[\mathbf{n}'\times\mathcal{E}_0]\times\mathbf{n}'$$
$$\left.\left.\times n(\mathbf{r},t)e^{i\mathbf{k}_0\cdot\mathbf{r}}e^{-i\omega_0 t}d^3\mathbf{r}\right]d^2\mathbf{r}'\right\}, \quad (19)$$

where we have inserted Eqs. (14) and (13) for the LO and scattered electric field, respectively. We now introduce the Fresnel-Kirchhoff diffraction formula

$$\frac{1}{i\lambda_0}\int_A\frac{e^{ik_0|\mathbf{r}'-\mathbf{r}|}}{|\mathbf{r}'-\mathbf{r}|}u^*_{LO}(\mathbf{r}')\mathcal{E}^*_{LO}e^{-ik_0\mathbf{n}'\cdot\mathbf{r}'}d^2\mathbf{r}' = u^*_{LO}(\mathbf{r})\mathcal{E}^*_{LO}e^{-i\mathbf{k}_s\cdot\mathbf{r}}, \quad (20)$$

which is the radiated field for small angles of diffraction from a known monochromatic field distribution on a diaphragm A [33]. This radiated field (the antenna or virtual LO beam [29]) propagates from the detector to the scatterers [34]. The reciprocity theorem of Helmholtz states that a point source at $\mathbf{r}$ will produce at $\mathbf{r}'$ the same effect as a point source of equal intensity placed at $\mathbf{r}'$ will produce at $\mathbf{r}$ [33]. Therefore Eq. (20) describing the field in the measurement volume (position $\mathbf{r}$) due to a source at the detector (position $\mathbf{r}'$) is equivalent to the reverse situation, where the measurement volume is the source.

In Eq. (21) we first reorganize Eq. (19) and then apply the Fresnel-Kirchhoff diffraction formula

$$i_k(t)\frac{\hbar\omega_0}{e\eta} = 2Re\left\{\frac{k_0^2\alpha_0}{4\pi}\frac{1}{\mu_0 c}e^{it\omega_\Delta}\right.$$
$$\times\int_V\left[\frac{i\lambda_0}{i\lambda_0}\int_A\frac{e^{ik_0|\mathbf{r}'-\mathbf{r}|}}{|\mathbf{r}'-\mathbf{r}|}u^*_{LO}(\mathbf{r}')\mathcal{E}^*_{LO}e^{-i\mathbf{k}_s\cdot\mathbf{r}'}d^2\mathbf{r}'\right]$$
$$\left.\times[\mathbf{n}'\times\mathcal{E}_0]\times\mathbf{n}'e^{i\mathbf{k}_0\cdot\mathbf{r}}u_0(\mathbf{r})n(\mathbf{r},t)d^3\mathbf{r}\right\}$$
$$= 2Re\left\{i\frac{k_0^2\alpha_0}{4\pi}\frac{\lambda_0}{\mu_0 c}e^{it\omega_\Delta}\right.$$
$$\left.\times\int_V\mathcal{E}^*_{LO}u^*_{LO}(\mathbf{r})e^{-i\mathbf{k}_s\cdot\mathbf{r}}\mathcal{E}_0u_0(\mathbf{r})e^{i\mathbf{k}_0\cdot\mathbf{r}}n(\mathbf{r},t)d^3\mathbf{r}\right\}$$
$$= 2Re\left\{i\frac{\pi\alpha_0}{\lambda_0}\sqrt{\frac{\varepsilon_0}{\mu_0}}e^{it\omega_\Delta}\int_V\mathcal{E}^*_{LO}u^*_{LO}(\mathbf{r})\mathcal{E}_0u_0(\mathbf{r})e^{-i\mathbf{k}\cdot\mathbf{r}}n(\mathbf{r},t)d^3\mathbf{r}\right\}, \quad (21)$$

since

$$\frac{k_0^2\alpha_0}{4\pi}\frac{\lambda_0}{\mu_0 c} = \frac{\pi\alpha_0}{\lambda_0}\sqrt{\frac{\varepsilon_0}{\mu_0}} \quad (22)$$

and

$$[\mathbf{n}'\times\mathcal{E}_0]\times\mathbf{n}' = \mathcal{E}_0 \quad (23)$$

The expression for the current now becomes

$$i_k(t) = 2\frac{e\eta}{\hbar\omega_0}\sqrt{\frac{\varepsilon_0}{\mu_0}}\lambda_0$$
$$\times Re\left\{ir_e e^{i\omega_\Delta t}\mathcal{E}_0\mathcal{E}^*_{LO}\int_V n(\mathbf{r},t)u_0(\mathbf{r})u^*_{LO}(\mathbf{r})e^{-i\mathbf{k}\cdot\mathbf{r}}d^3\mathbf{r}\right\}, \quad (24)$$

where $\mathcal{E}^*_{LO}$ and $\mathcal{E}_0$ hereafter are to be considered as scalars since the laser field and the LO field are assumed to have identical polarization.

We introduce a shorthand notation for the spatial Fourier transform

$$(n(t)U)_k = \int_V n(\mathbf{r},t)U(\mathbf{r})e^{-i\mathbf{k}\cdot\mathbf{r}}d^3\mathbf{r}$$
$$U(\mathbf{r}) = u_0(\mathbf{r})u^*_{LO}(\mathbf{r}), \quad (25)$$

where U is called the beam profile [29, 34]. We note that

$$\int_V n(\mathbf{r},t)U(\mathbf{r})e^{-i\mathbf{k}\cdot\mathbf{r}}d^3\mathbf{r} = \int n(\mathbf{k}',t)U(\mathbf{k}-\mathbf{k}')\frac{d^3\mathbf{k}'}{(2\pi)^3}$$
$$= n(\mathbf{k},t)\star U(\mathbf{k})$$

$$n(\mathbf{k},t) = \int_V n(\mathbf{r},t)e^{-i\mathbf{k}\cdot\mathbf{r}}d^3\mathbf{r}$$
$$U(\mathbf{k}) = \int_V U(\mathbf{r})e^{-i\mathbf{k}\cdot\mathbf{r}}d^3\mathbf{r}, \quad (26)$$

where $\star$ denotes convolution [31, 35]. We arrive at

$$i_k(t) = 2\frac{e\eta}{\hbar\omega_0}\sqrt{\frac{\varepsilon_0}{\mu_0}}\lambda_0 Re[ir_e e^{i\omega_\Delta t}\mathcal{E}_0\mathcal{E}^*_{LO}(n(t)U)_k] \quad (27)$$

Defining

$$\gamma = \frac{e\eta}{\hbar\omega_0}\sqrt{\frac{\varepsilon_0}{\mu_0}}\lambda_0 r_e\mathcal{E}_0\mathcal{E}^*_{LO}, \quad (28)$$

Eq. (24) in its final guise is

$$i_k(t) = i[\gamma e^{i\omega_\Delta t}(n(t)U)_k - \gamma^* e^{-i\omega_\Delta t}(n(t)U)^*_k] \quad (29)$$

Note that the $e^{-i\mathbf{k}\cdot\mathbf{r}}$ term in $(n(t)U)_k$ constitutes a spatial band pass filter ($\mathbf{k}$ is fixed). Three scales are involved [36]:

- Fluctuations occur at scales r much smaller than $\lambda = 2\pi/k \Rightarrow \mathbf{k}\cdot\mathbf{r} \ll 1 \Rightarrow e^{-i\mathbf{k}\cdot\mathbf{r}} \approx 1$. The Fourier transform becomes the mean value of the density fluctuations, which is zero.
- Fluctuations occur at scales r similar to $\lambda = 2\pi/k$; this leads to the main contribution to the signal.
- Fluctuations occur at scales r much larger than $\lambda = 2\pi/k \Rightarrow \mathbf{k}\cdot\mathbf{r} \gg 1 \Rightarrow e^{-i\mathbf{k}\cdot\mathbf{r}}$ is highly oscillatory. The mean value will be roughly equal to that of $e^{-i\mathbf{k}\cdot\mathbf{r}}$, which is zero.

The scattered power P_k resulting from the interference term can be written by defining a constant

$$\xi = \sqrt{\frac{\varepsilon_0}{\mu_0}}\lambda_0 r_e\mathcal{E}_0\mathcal{E}^*_{LO} \quad (30)$$

and replacing γ with this in Eq. (29)

$$P_k(t) = \frac{\hbar\omega_0}{e\eta}i_k(t) = i[\xi e^{i\omega_\Delta t}(n(t)U)_k - \xi^* e^{-i\omega_\Delta t}(n(t)U)^*_k]$$
$$= 2Re[i\xi e^{i\omega_\Delta t}(n(t)U)_k] \quad (31)$$

If $\mathcal{E}_0$ and $\mathcal{E}_{LO}$ are real numbers (meaning that ξ is real) we can go one step further and write

$$P_k(t) = 2\xi Re[ie^{i\omega_\Delta t}(n(t)U)_k]$$
$$= 8\frac{\lambda_0 r_e}{\pi w^2}\sqrt{P_0 P_{LO}}Re[ie^{i\omega_\Delta t}(n(t)U)_k] \quad (32)$$

assuming that $P_{0/LO} = \frac{\pi w^2}{4}\sqrt{\frac{\varepsilon_0}{\mu_0}}|\mathcal{E}^2_{0/LO}|$ (for a given U, see section II G 2).

E. Demodulation

The task now is to extract real and imaginary parts of $(n(t)U)_k$. We construct two signals that are shifted by $\pi/2$ [37]

$$j_1(t) = Re[e^{i\omega_\Delta t}] = \cos(\omega_\Delta t)$$
$$j_2(t) = Re[e^{i(\omega_\Delta t+\pi/2)}] = \sin(\omega_\Delta t) \quad (33)$$

Now two quantities are constructed using Eqs. (29) (divided into two equal parts) and (33)

$$\begin{aligned} i_{d,1} &= \frac{i_k(t)}{2} j_1(t) \\ &= \frac{i}{4}[\gamma e^{i2\omega_\Delta t}(n(t)U)_k + \gamma(n(t)U)_k - \gamma^*(n(t)U)_k^* \\ &\quad -\gamma^* e^{-i2\omega_\Delta t}(n(t)U)_k^*] \\ i_{d,2} &= \frac{i_k(t)}{2} j_2(t) \\ &= \frac{i}{4}[\gamma e^{i2\omega_\Delta t}e^{i\pi/2}(n(t)U)_k+\gamma e^{-i\pi/2}(n(t)U)_k - \gamma^* e^{i\pi/2}(n(t)U)_k^* \\ &\quad -\gamma^* e^{-i2\omega_\Delta t}e^{-i\pi/2}(n(t)U)_k^*] \end{aligned} \quad (34)$$

Low pass filtering (LPF) of these quantities removes the terms containing the fast $2\omega_\Delta$ expression [38]. The result is that

$$\begin{aligned} i_{d,complex} &= [i_{d,2} - i i_{d,1}]_{LPF} \\ &= \tfrac{1}{2}(Re[\gamma(n(t)U)_k] - i(-Im[\gamma(n(t)U)_k])) \\ &= \tfrac{\gamma}{2}(n(t)U)_k \end{aligned} \quad (35)$$

Now we have $(n(t)U)_k$ and can analyze this complex quantity using spectral tools. The alternative to heterodyne detection is called homodyne detection. There are two advantages that heterodyne detection has compared to homodyne detection [36]:

1. The LO beam provides an amplification factor to the detected signal (see Eq. (32)).
2. It leaves the complex $(n(t)U)_k$ intact multiplied by a wave having frequency ω_Δ; in homodyne detection the electric field complex number is transformed into a real number and the phase information is lost. The frequency sign of the scattered power tells us in which direction the fluctuations are moving.

F. Phase separation

Since the theory behind phase separation is extensively described in section 2 of Ref. 39, we will here only give a brief recapitulation of the basics.

The observed signal is interpreted as being due to a large number of 'electron bunches', each moving in a given direction. An electron bunch is defined as a collection of electrons occupying a certain region of the measurement volume V. This definition is motivated by the fact that even though the measurement volume includes a large number of cells (V/λ^3) [40] (typically ~3000 in W7-AS), the amplitude of the signal consists of both large and small values separated in time. The demodulated photocurrent $i_{d,complex}$ is a complex number; it can be written

$$i_{d,complex}(t) = \sum_{j=1}^{N_b} a_j e^{i\phi_j} = A e^{i\Phi}, \quad (36)$$

where N_b is the number of bunches, while a_j and ϕ_j is the amplitude and phase of bunch number j, respectively. The criterion for determination of direction is

$$\begin{aligned} &\partial_t \Phi > 0 \Rightarrow \mathbf{k}\cdot\mathbf{U} > 0 \Rightarrow \text{fluctuations} \parallel \mathbf{k} \\ &\partial_t \Phi < 0 \Rightarrow \mathbf{k}\cdot\mathbf{U} < 0 \Rightarrow \text{fluctuations} \parallel -\mathbf{k}, \end{aligned} \quad (37)$$

where $\Phi = \mathbf{k}\cdot\mathbf{U}t$ and $\mathbf{U}$ is the average bunch velocity. The phase derivative sign reflects the bunches with highest intensities occurring most frequently.

G. Density fluctuations

1. Derivation. The current frequency spectral density measured is

$$I_k(\omega) = \frac{|i_k(\omega)|^2}{T}$$
$$i_k(\omega) = \int_{t_1}^{t_2} e^{i\omega t} i_k(t) dt = \int^T e^{i\omega t} i_k(t)\, dt, \quad (38)$$

where $T = t_2 - t_1$ is a time interval. Using Eq. (29) this can be written

$$I_k(\omega) = \frac{|\gamma^2|}{T}\{|(n(\omega)U)_k|^2 + |(n(-\omega)U)_k|^2\}$$
$$(n(\omega)U)_k = \int d^3\mathbf{r} \int^T n(\mathbf{r},t)U(\mathbf{r})e^{i(\omega t-\mathbf{k}\cdot\mathbf{r})} dt$$
$$n(\mathbf{k},\omega) = \int^T n(\mathbf{k},t)e^{i\omega t} dt, \quad (39)$$

assuming that $n(\mathbf{k},\omega)$ and $n(\mathbf{k},-\omega)$ are independent (i.e. no mixed terms) [29]. Note that we have dropped the ω_Δ terms; it has previously been explained how we filter these high frequencies away. Now we are approaching an analytical expression for the weighted mean square density fluctuations. The time fluctuating part of $n(\mathbf{r},t)$ is

$$\delta n(\mathbf{r},t) = n(\mathbf{r},t) - \frac{1}{T}\int^T n(\mathbf{r},t)\, dt \quad (40)$$

When δn is written without a subscript, it is taken to refer to the electron density fluctuations. Eq. (40) enables us to express the weighted mean square density fluctuations as

$$\langle \delta n^2 \rangle_{UT} = \frac{\int^T dt \int \delta n^2(\mathbf{r},t)|U(\mathbf{r})|^2\, d^3\mathbf{r}}{T\int |U(\mathbf{r})|^2\, d^3\mathbf{r}} \quad (41)$$

The subscript means averaging over the beam profile $U(\mathbf{r})$ and a time interval T. We can transform this via Parseval's theorem

$$\int^T dt \int |\delta n(\mathbf{r},t)U(\mathbf{r})|^2 d^3\mathbf{r} = \int \frac{d\omega}{2\pi}\int \frac{d^3\mathbf{k}}{(2\pi)^3}|(\delta n(\omega)U)_k|^2 \quad (42)$$

to the wave vector-frequency domain

$$\langle \delta n^2 \rangle_{UT} = n_0 \int \frac{d\omega}{2\pi}\int \frac{d^3\mathbf{k}}{(2\pi)^3} S_U(\mathbf{k},\omega)$$
$$S_U(\mathbf{k},\omega) = \frac{|(\delta n(\omega)U)_k|^2}{n_0 T\int |U(\mathbf{r})|^2\, d^3\mathbf{r}}, \quad (43)$$

where n_0 is the mean density in the scattering volume. $S_U(\mathbf{k},\omega)$ is the measured spectral density also known as the form factor. Conventionally, this is given as

$$S(\mathbf{k},\omega) = \frac{|\delta n(\mathbf{k},\omega)|^2}{n_0 VT}$$
$$\delta n(\mathbf{r},t) = \int \frac{d\omega}{2\pi}\int \frac{d^3\mathbf{k}}{(2\pi)^3}\delta n(\mathbf{k},\omega)e^{-i(\omega t-\mathbf{k}\cdot\mathbf{r})} \quad (44)$$

Combining Eqs. (43) and (39) (replacing n by δn) we get

$$S_U(\mathbf{k},\omega,-\omega) = S_U(\mathbf{k},\omega) + S_U(\mathbf{k},-\omega) = \frac{I_k(\omega)}{n_0|\gamma^2|\int|U(\mathbf{r})|^2\mathrm{d}^3\mathbf{r}} \quad (45)$$

The term with positive frequency corresponds to density fluctuations propagating in the **k**-direction, while negative frequency means propagation in the opposite direction [16].

The wavenumber resolution width is

$$\Delta k^3 = \left[\int |U(\mathbf{r})|^2\,\mathrm{d}^3\mathbf{r}\right]^{-1} \quad (46)$$

We have now arrived at the goal; replacing $S_U(\mathbf{k},\omega)$ by $S_U(\mathbf{k},\omega,-\omega)$ in the first line of Eq. (43), our final expression for the mean square density fluctuations is

$$\langle\delta n^2\rangle_{UT} = \int \frac{\mathrm{d}^3\mathbf{k}}{(2\pi)^3}\frac{\langle\delta n^2\rangle_k}{\Delta k^3}$$

$$\langle\delta n^2\rangle_k = \frac{1}{|\gamma^2|\left[\int|U(\mathbf{r})|^2\mathrm{d}^3\mathbf{r}\right]^2}\int_{-\infty}^{\infty}\frac{\mathrm{d}\omega}{2\pi}I_k(\omega) \quad (47)$$

The frequency integration is done numerically, while a wavenumber integration can be done by measuring I_k for different wavenumber values.

2. An example. When the beam profile $U(\mathbf{r})$ is known, quantitative expressions for the density fluctuations can be calculated [29]. The following assumptions are made:

- Antenna beam corresponds to LO beam.
- Beams have Gaussian profiles.
- Beams are focused in the measurement region with identical waists w.
- Forward scattering.

Furthermore, the beam profile $U(\mathbf{r})$ is assumed to be

$$\begin{aligned} U(\mathbf{r}) &= u_0(\mathbf{r})u^*_{\mathrm{LO}}(\mathbf{r}) = e^{-2(x^2+y^2)/w^2} \quad \text{for } |z| < L/2 \\ U(\mathbf{r}) &= 0 \qquad\qquad\qquad\qquad\quad \text{for } |z| > L/2, \end{aligned} \quad (48)$$

where L is the measurement volume length and the beams are along z.

The wavenumber resolution width Δk^3 becomes $4/(\pi w^2 L)$ and we find the wavenumber resolution itself by calculating

$$\begin{aligned} U(\mathbf{k}) &= \int_V U(\mathbf{r})e^{-\mathrm{i}\mathbf{k}\cdot\mathbf{r}}\,\mathrm{d}^3\mathbf{r} \\ &= \int_{-L/2}^{L/2} e^{-\mathrm{i}k_z z}\,\mathrm{d}z\left[\int_{-\infty}^{\infty} e^{-\left(\frac{2}{w^2}x^2+\mathrm{i}k_x x\right)}\mathrm{d}x\right] \\ &\quad\times\left[\int_{-\infty}^{\infty} e^{-\left(\frac{2}{w^2}y^2+\mathrm{i}k_y y\right)}\mathrm{d}y\right] \\ &= \frac{2}{k_z}\sin\left(\frac{k_z L}{2}\right)\left[\sqrt{\frac{\pi}{2}}we^{-\frac{k_x^2w^2}{8}}\right]\left[\sqrt{\frac{\pi}{2}}we^{-\frac{k_y^2w^2}{8}}\right], \end{aligned} \quad (49)$$

allowing us to define the transverse wavenumber resolutions $\Delta k_{x,y} = 2/w$ (e^{-1} value [34]) and a longitudinal wavenumber resolution $\Delta k_z = 2\pi/L$ (sine term zero) [16]. We further obtain an expression for the main (and LO) beam power

$$P_0 = \sqrt{\frac{\varepsilon_0}{\mu_0}}\int_{-\infty}^{\infty}|\mathcal{E}_0^2|e^{-\frac{4(x^2+y^2)}{w^2}}\,\mathrm{d}x\,\mathrm{d}y = \frac{\pi w^2}{4}\sqrt{\frac{\varepsilon_0}{\mu_0}}|\mathcal{E}_0^2|, \quad (50)$$

$$I_n = \frac{e^2\eta P_{\mathrm{LO}}}{\hbar\omega_0} \quad \text{and} \quad P_{\mathrm{LO}} = \frac{\pi w^2}{4}\sqrt{\frac{\varepsilon_0}{\mu_0}}|\mathcal{E}^2_{\mathrm{LO}}|.$$

Using Eq. (47) for this example we get

$$\begin{aligned} \langle\delta n^2\rangle_k &= \frac{1}{(2\pi)^3}\left(\frac{\hbar\omega_0}{\mathrm{e}\eta}\right)^2\frac{1}{\lambda_0^2 r_{\mathrm{e}}^2 L^2}\frac{1}{P_0 P_{\mathrm{LO}}}\int_{-\infty}^{\infty}\frac{\mathrm{d}\omega}{2\pi}I_k(\omega) \\ &= \frac{1}{(2\pi)^3}\frac{\hbar\omega_0}{\eta}\frac{1}{\lambda_0^2 r_{\mathrm{e}}^2 L^2}\frac{1}{P_0}\int_{-\infty}^{\infty}\frac{\mathrm{d}\omega}{2\pi}\frac{I_k(\omega)}{I_n} \end{aligned} \quad (51)$$

This example concludes our section on the theory of collective light scattering. In section II D we derived the analytical expression for the photocurrent, enabling us to interpret the signal as a spatial Fourier transform of density multiplied by the beam profile. In the present section this result was used to deduce an equation for δn^2 (Eq. (47)).

III. Spatial Localization

In this section we first investigate the geometry of the measurement volume (section III A). Thereafter we explore the possibilities of obtaining localized measurements; first using a simple method directly limiting the volume length (section III B) and then by assuming that the density fluctuations have certain properties (section III C).

A. The measurement volume

1. Geometrical estimate. A measurement volume is created by interference between the incoming main (M) beam (wave vector $\mathbf{k}_0$) and the local oscillator (LO) beam (wave vector $\mathbf{k}_s$), see Fig. 2.

The angle between the LO and M beams is called the scattering angle θ_s. The distance between the interference fringes [38] is

$$\lambda_{\mathrm{geom}} = \frac{\lambda_0}{2\sin\left(\frac{\theta_s}{2}\right)} \approx \frac{\lambda_0}{\theta_s} \quad (52)$$

The scattering angle determines the measured wavenumber [16]

$$k = 2k_0\sin\left(\frac{\theta_s}{2}\right) \approx k_0\theta_s \qquad \lambda = \frac{2\pi}{k} \qquad k \ll k_0 \quad (53)$$

The approximations above are valid for small scattering angles. Assuming that the beams have identical diameters $2w$, the volume length can be estimated as

$$L_{\mathrm{geom}} = \frac{2w}{\tan\left(\frac{\theta_s}{2}\right)} \approx \frac{4w}{\theta_s} \quad (54)$$

The fringe number, i.e. the number of wavelengths that can be fitted into the measurement volume, is

$$M = \frac{2w}{\lambda} = \frac{wk}{\pi} \quad (55)$$

2. Exact result. The time-independent field from each of the two Gaussian beams creating a measurement volume can be written

$$u(\mathbf{r}) = u(x,y,z) = \sqrt{\frac{2P}{\pi w^2(z)}}e^{-\frac{x^2+y^2}{w^2(z)}+\mathrm{i}k_0 z\left(1+\frac{x^2+y^2}{2(z_R^2+z^2)}\right)+\mathrm{i}\phi(z)} \quad (56)$$

Here, P is the beam power,

$$w(z) = w_0\sqrt{1+\left(\frac{z}{z_R}\right)^2} \quad (57)$$

is the beam radius at z and z_R is the Rayleigh range

$$z_R = \frac{\pi w_0^2}{\lambda_0}, \quad (58)$$

which is the distance from the waist w_0 to where the beam radius has grown by a factor $\sqrt{2}$. Note that we have introduced the beam waist w_0 and the Rayleigh range explicitly for the following calculations. The phase is given by

$$\phi(z) = \arctan\left(\frac{z_R}{z}\right) \tag{59}$$

We use the complete Gaussian description here instead of the simple form used in section II.

An excellent treatment of the measurement volume has been given in Ref. 38; therefore we will here restrict ourselves to simply quoting the important results and approximations in sections III A 2a and III A 2b.

a. Intensity. We now want to find an expression for the interference power in the measurement volume. Since the full angle between the LO and M beams is θ_s, we will construct two new coordinate systems, rotated $\pm\theta_s/2$ around the y-axis. We define the constants

$$c = \cos\left(\frac{\theta_s}{2}\right) \qquad s = \sin\left(\frac{\theta_s}{2}\right) \tag{60}$$

and use them to construct the two transformations from the original system

$$x_0 = cx - sz \qquad y_0 = y \qquad z_0 = sx + cz \tag{61}$$

and

$$x_{\mathrm{LO}} = cx + sz \qquad y_{\mathrm{LO}} = y \qquad z_{\mathrm{LO}} = -sx + cz \tag{62}$$

This enables us to use Eq. (56) for each beam in the rotated systems. The intensity distribution in rotated coordinates can be written

$$|u_0 u_{\mathrm{LO}}^*| = \frac{2\sqrt{P_0 P_{\mathrm{LO}}}}{\pi w(z_0) w(z_{\mathrm{LO}})} e^{-\frac{w^2(z_{\mathrm{LO}})\left[x_0^2+y_0^2\right]+w^2(z_0)\left[x_{\mathrm{LO}}^2+y_{\mathrm{LO}}^2\right]}{w^2(z_0)w^2(z_{\mathrm{LO}})}} \tag{63}$$

The intensity distribution in the original coordinate system can now be found by inserting the transformations (61) and (62) into Eq. (63). A few approximations lead to the following expression

$$|u_0 u_{\mathrm{LO}}^*| = \frac{2\sqrt{P_0 P_{\mathrm{LO}}}}{\pi w_0^2}\left(1 + \frac{c^2 z^2}{z_R^2}\right)^{-1} e^{-\frac{2(1+c^2z^2/z_R^2)(c^2x^2+y^2+s^2z^2)+8(csxz/z_R)^2}{w_0^2(1+c^2z^2/z_R^2)^2}} \tag{64}$$

Here, the terms including z_R are due to beam divergence effects. Eq. (64) can be integrated over the (x, y)-plane to obtain the variation of the interference power as a function of z

$$\begin{aligned} P(z) &= \int\int \mathrm{d}x\,\mathrm{d}y |u_0 u_{\mathrm{LO}}^*| \\ &= \frac{\sqrt{P_0 P_{\mathrm{LO}}}}{c}\left(\frac{1 + c^2 z^2/z_R^2}{1 + (1+3s^2)z^2/z_R^2}\right)^{1/2} e^{-\frac{2s^2z^2}{w_0^2(1+c^2z^2/z_R^2)}} \end{aligned} \tag{65}$$

For small scattering angles,

$$c \approx 1 \qquad s \approx \frac{\theta_s}{2}, \tag{66}$$

meaning that the z-dependent pre-factor in Eq. (65) is close to unity for $z \le z_R$. Therefore the behaviour of $P(z)$ can be gauged from the exponential function. We define the position z_a where the power has fallen to a times its maximum value

$$P(z_a) = aP(0) \tag{67}$$

The z_a-position is now inserted into the exponential function of Eq. (65)

$$\begin{aligned} a &= e^{-\frac{2s^2z_a^2}{w_0^2(1+c^2z_a^2/z_R^2)}} \\ z_a &= \pm\sqrt{\frac{\ln(1/a)}{2}}\frac{w_0}{s}\left(1 + \frac{\ln a}{2}\left(\frac{cw_0}{sz_R}\right)^2\right)^{-1/2} \end{aligned} \tag{68}$$

The measurement volume length can now be defined as

$$\begin{aligned} L_{\mathrm{exact}} &= 2|z_{e^{-2}}| = \frac{2w_0}{s}\left(1 - \left(\frac{cw_0}{sz_R}\right)^2\right)^{-1/2} \\ &\approx \frac{4w_0}{\theta_s}\left(1 - \left(\frac{4}{\pi M}\right)^2\right)^{-1/2} \end{aligned} \tag{69}$$

The correction from the geometrical estimate (54) can be estimated by assuming that $M \ge 2$; this means that the correction factor

$$\left(\frac{4}{\pi M}\right)^2 \le \frac{4}{\pi^2} \tag{70}$$

The increase of the measurement volume length from the geometrical estimate is due to the divergence of the Gaussian beams.

As a final point, we can compare the beam divergence angle θ_d to the scattering angle θ_s

$$\theta_d = \frac{\lambda_0}{\pi w_0} = \frac{w_0}{z_R} = \frac{2\theta_s}{\pi M} \tag{71}$$

A large M means that $\theta_d \ll \theta_s$, so that the beams will separate as one moves away from $z = 0$.

b. Phase. The phase of the interference in rotated coordinates is given by

$$e^{\left[\mathrm{i}k_0\left(z_0 - z_{\mathrm{LO}} + \frac{z_0\left[x_0^2+y_0^2\right]}{2\left[z_R^2+z_0^2\right]} - \frac{z_{\mathrm{LO}}\left[x_{\mathrm{LO}}^2+y_{\mathrm{LO}}^2\right]}{2\left[z_R^2+z_{\mathrm{LO}}^2\right]}\right) + \mathrm{i}(\phi(z_0) - \phi(z_{\mathrm{LO}}))\right]} \tag{72}$$

Neglecting the $(\phi(z_0) - \phi(z_{\mathrm{LO}}))$-term and inserting the original coordinates, the fringe distance is

$$\begin{aligned} \lambda_{\mathrm{exact}} &= \frac{\lambda_0}{2s[1+\delta(z)]} \approx \frac{\lambda_0}{\theta_s[1+\delta(z)]} \\ \delta(z) &= \frac{(1-3c^2)z_R^2 z^2 - (1+c^2)c^2 z^4}{2(z_R^2 + c^2 z^2)^2} \approx -\frac{z^2}{z_R^2 + z^2} \end{aligned} \tag{73}$$

The exact expression for the fringe distance has a correction term $\delta(z)$ compared to the geometrical estimate in Eq. (52). For example, if $z = z_R/2$, δ is equal to -0.2, meaning a 25% increase of the fringe distance. But of course the power in the interference pattern $P(z)$ decreases rapidly as well.

B. Direct localization

From Eq. (54) we immediately see that spatial localization along the measurement volume can be achieved by having a large scattering angle (large k). We will call this method direct localization, since the measurement volume is small in the z direction.

To localize along the beams, the measurement volume length L_{geom} must be much smaller than the plasma diameter $2a$, where a is the minor radius of the plasma.

Assuming that $a = 0.3\,\text{m}$, $w = 0.01\,\text{m}$ and that we want L_{geom} to be 0.2 m, the scattering angle θ_s is 11° (or 199 mrad). This corresponds to a wavenumber k of $1180\,\text{cm}^{-1}$.

However, measurements show that the scattered power decreases very fast with increasing wavenumber, either as a power-law or even exponentially. This means that with our detection system, we have investigated a wavenumber range of $[14, 62]\,\text{cm}^{-1}$. For this interval, the measurement volume is much longer than the plasma diameter, meaning that the measurements are integrals over the entire plasma cross section.

C. Indirect localization

We stated above that the measured fluctuations are line integrated along the entire plasma column because the scattering angle is quite small (of order 0.3° or 5 mrad). However, the possibility to obtain localized measurements still exists, albeit indirect localization. For this method to work, we use the fact that the density fluctuation wavenumber κ is anisotropic in the directions parallel and perpendicular to the local magnetic field in the plasma. This method was experimentally demonstrated in the Tore Supra tokamak using the ALTAIR diagnostic [16].

The section is organized as follows: In section III C 1 we introduce the dual volume geometry and the definition of the magnetic pitch angle. Thereafter we derive an analytical expression for the crosspower between the volumes and finally describe issues concerning the correlation between spatially separated measurement volumes. In section III C 2 we describe the single volume geometry and present a simplified formula for the autopower. A few assumptions are introduced, allowing us to simulate the expression for the autopower. In section III C 3 we compare the dual and single volume localization criteria found in the two initial sections.

1. Dual volume

a. Dual volume geometry. The geometry belonging to the dual volume setup is shown in Fig. 3. The left-hand plot shows a simplified version of the optical setup and the right-hand plot shows the two volumes as seen from above. The size of the vector $\mathbf{d}$ connecting the two volumes is constant for a given setup, whereas the angle $\theta_R = \arcsin(d_R/d)$ can be varied. The length d_R is the distance between the volumes along the major radius R. The wave vectors selected by the diagnostic ($\mathbf{k}_1$ and $\mathbf{k}_2$) and their angles with respect to R (α_1 and α_2) have indices corresponding to the volume number, but are identical for our diagnostic.

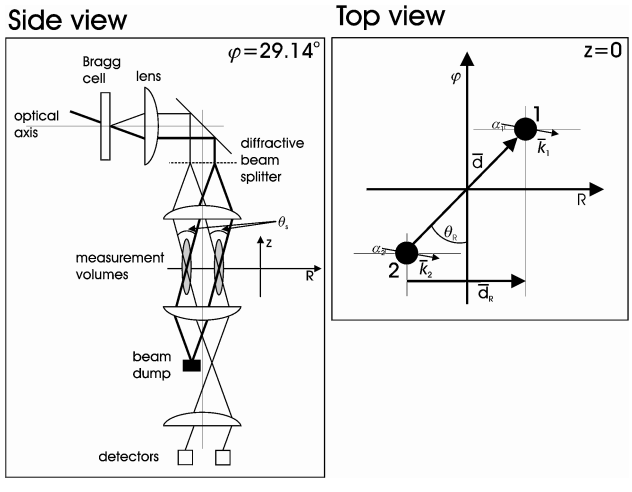

Fig. 3. Left: Schematic representation of the dual volume setup (side view). Thick lines are the M beams, thin lines the LO beams, right: The dual volume setup seen from above. The black dots are the measurement volumes.

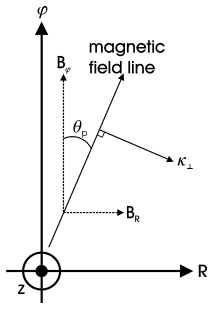

Fig. 4. Geometry of a magnetic field line for fixed z.

b. The magnetic pitch angle. The main component of the magnetic field is the toroidal magnetic field, B_φ. The small size of the magnetic field along R, B_R, implies that a magnetic field line is not completely in the toroidal direction, but also has a poloidal part. The resulting angle is called the pitch angle θ_p, see Fig. 4.

The pitch angle is defined to be

$$\theta_p^{\text{def}} = \arctan\left(\frac{B_\theta}{B_\varphi}\right), \tag{74}$$

which for fixed z (as in Fig. 4) becomes

$$\theta_p = \arctan\left(\frac{B_R}{B_\varphi}\right) \tag{75}$$

As one moves along a measurement volume from the bottom to the top of the plasma (thereby changing z), the ratio B_R/B_φ changes, resulting in a variation of the pitch angle θ_p. The central point now is that we assume that the fluctuation wavenumber parallel to the magnetic field line ($\kappa_\parallel$) is much smaller than the wavenumber perpendicular to the field line ($\kappa_\perp$)

$$\kappa_\parallel \ll \kappa_\perp \tag{76}$$

This case is illustrated in Fig. 4, where only the $\kappa_\perp$ part of the fluctuation wave vector $\boldsymbol{\kappa}$ is shown. It is clear that when θ_p changes, the direction of $\kappa_\perp$ will vary as well [16].

c. Localized crosspower. Below we will derive an expression for the scattered crosspower between two measurement volumes (Eq. (95)). The derivation is based on work presented in Ref. 37. We will ignore constant factors and thus only do proportionality calculations to arrive at the integral. This equation will prove to be crucial for the understanding of the observed signal and the limits imposed on localization by the optical setup.

The wave vectors used for the derivation are shown in Fig. 5. The size and direction of the wave vectors $\mathbf{k}_1$ and $\mathbf{k}_2$ are allowed to differ. The positions of the measurement volumes are $\mathbf{r}$ (volume 1) and $\mathbf{r}'$ (volume 2). We assume that d is zero (see Fig. 3); effects associated with a spatial separation of the volumes are discussed after the derivation.

We introduce a few additional definitions that will prove to be useful; the difference between the two measured wave vectors $\mathbf{k}_d$,

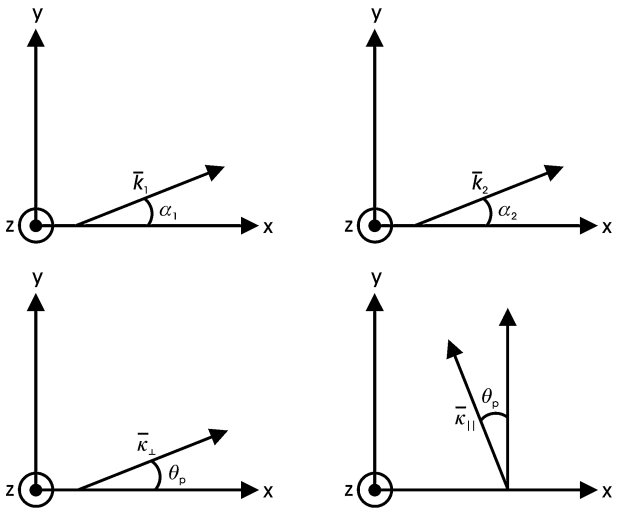

Fig. 5. Wave vectors in rectangular coordinates. Top left: $\mathbf{k}_1 = (k_1 \cos\alpha_1, k_1 \sin\alpha_1, 0)$, top right: $\mathbf{k}_2 = (k_2 \cos\alpha_2, k_2 \sin\alpha_2, 0)$, bottom: $\boldsymbol{\kappa} = (\kappa_\perp \cos\theta_p - \kappa_\parallel \sin\theta_p, \kappa_\perp \sin\theta_p + \kappa_\parallel \cos\theta_p, \kappa_{\perp_z})$.

the vector $\mathbf{R}$ and the difference in volume position $\boldsymbol{\rho}$

$$\mathbf{k}_d = \mathbf{k}_1 - \mathbf{k}_2 = (k_d \cos\beta, k_d \sin\beta, 0)$$
$$\mathbf{R} = \mathbf{r} = (X, Y, Z)$$
$$\boldsymbol{\rho} = \mathbf{r} - \mathbf{r}' = (x, y, z) \tag{77}$$

***

Our starting point is the current spectral density (Eq. (39))

$$I_{12}(\mathbf{k}_1, \mathbf{k}_2, \omega) \propto \int \mathrm{d}\mathbf{r} \int \mathrm{d}\mathbf{r}' \langle n(\mathbf{r}, \omega) n^*(\mathbf{r}', \omega)\rangle \times U_1(\mathbf{r}) U_2^*(\mathbf{r}') e^{\mathrm{i}\mathbf{k}_1\cdot\mathbf{r}} e^{-\mathrm{i}\mathbf{k}_2\cdot\mathbf{r}'}, \tag{78}$$

where $\langle\cdot\rangle$ is a temporal average. Since

$$\mathbf{k}_1 \cdot \mathbf{r} - \mathbf{k}_2 \cdot \mathbf{r}' = \mathbf{k}_d \cdot \mathbf{R} + \mathbf{k}_2 \cdot \boldsymbol{\rho} \tag{79}$$

we can rewrite Eq. (78) using the substitution $\boldsymbol{\rho} = \mathbf{r} - \mathbf{r}'$ to become

$$I_{12}(\mathbf{k}_1, \mathbf{k}_2, \omega) \propto \int \mathrm{d}\mathbf{R} \int \mathrm{d}\boldsymbol{\rho} \langle n(\mathbf{R}, \omega) n^*(\mathbf{R} - \boldsymbol{\rho}, \omega)\rangle \times U_1(\mathbf{R}) U_2^*(\mathbf{R} - \boldsymbol{\rho}) e^{\mathrm{i}\mathbf{k}_d\cdot\mathbf{R}} e^{\mathrm{i}\mathbf{k}_2\cdot\boldsymbol{\rho}} \tag{80}$$

We define the local spectral density of the density fluctuations to be

$$S(\mathbf{k}_2, \mathbf{R}, \omega) = \int \mathrm{d}\boldsymbol{\rho} \langle n(\mathbf{R}, \omega) n^*(\mathbf{R} - \boldsymbol{\rho}, \omega)\rangle e^{\mathrm{i}\mathbf{k}_2\cdot\boldsymbol{\rho}}, \tag{81}$$

where the inverse Fourier transform yields

$$\langle n(\mathbf{R}, \omega) n^*(\mathbf{R} - \boldsymbol{\rho}, \omega)\rangle \propto \int \mathrm{d}\boldsymbol{\kappa} e^{-\mathrm{i}\boldsymbol{\kappa}\cdot\boldsymbol{\rho}}\ S(\boldsymbol{\kappa}, \mathbf{R}, \omega) \tag{82}$$

This allows us to simplify Eq. (80)

$$I_{12}(\mathbf{k}_1, \mathbf{k}_2, \omega) \propto \int \mathrm{d}\mathbf{R} \int \mathrm{d}\boldsymbol{\rho} \int \mathrm{d}\boldsymbol{\kappa} S(\boldsymbol{\kappa}, \mathbf{R}, \omega) U(\mathbf{R}) U(\mathbf{R} - \boldsymbol{\rho}) e^{\mathrm{i}(\mathbf{k}_2 - \boldsymbol{\kappa})\cdot\boldsymbol{\rho}} e^{\mathrm{i}\mathbf{k}_d\cdot\mathbf{R}}, \tag{83}$$

where we have assumed that the two beam profiles U_1 and U_2^* are identical and equal to U. Further, we assume that they have the functional form that was used in section II, so that

$$U(\mathbf{R}) U(\mathbf{R} - \boldsymbol{\rho}) = e^{-\frac{2}{w^2}(2X^2 + 2Y^2 + x^2 + y^2 - 2xX - 2yY)} \tag{84}$$

We note that

$$\mathbf{k}_d \cdot \mathbf{R} = X k_d \cos\beta + Y k_d \sin\beta \tag{85}$$

and we assume that the local spectral density only varies along (and not across) the measurement volumes

$$S(\boldsymbol{\kappa}, \mathbf{R}, \omega) = S(\boldsymbol{\kappa}, Z, \omega) \tag{86}$$

Inserting Eqs. (84)–(86) into Eq. (83) we arrive at

$$\begin{aligned} I_{12}(\mathbf{k}_1, \mathbf{k}_2, \omega) &\propto \int \mathrm{d}Z \int \mathrm{d}\boldsymbol{\kappa} S(\boldsymbol{\kappa}, Z, \omega) \int \mathrm{d}x\, \mathrm{d}y\, \mathrm{d}z e^{\mathrm{i}(\mathbf{k}_2 - \boldsymbol{\kappa})\cdot\boldsymbol{\rho}} \\ &\quad \times \int \mathrm{d}X\, \mathrm{d}Y e^{-\frac{2}{w^2}(2X^2 + 2Y^2 + x^2 + y^2 - 2xX - 2yY)} e^{\mathrm{i}(X k_d \cos\beta + Y k_d \sin\beta)} \\ &\propto \int \mathrm{d}Z \int \mathrm{d}\boldsymbol{\kappa} S(\boldsymbol{\kappa}, Z, \omega) \int \mathrm{d}x\, \mathrm{d}y\, \mathrm{d}z\, e^{\mathrm{i}(\mathbf{k}_2 - \boldsymbol{\kappa})\cdot\boldsymbol{\rho}} \\ &\quad \times e^{-\frac{x^2}{w^2} + \frac{\mathrm{i}k_d x \cos\beta}{2}} e^{-\frac{y^2}{w^2} + \frac{\mathrm{i}k_d y \sin\beta}{2}} e^{-\frac{k_d^2 w^2}{16}}, \end{aligned} \tag{87}$$

where we have used that

$$\int_{-\infty}^{\infty} e^{-(ax^2 + bx + c)} \mathrm{d}x = \sqrt{\frac{\pi}{a}} e^{(b^2 - 4ac)/4a}$$
$$\int \mathrm{d}X e^{-\left(\frac{4}{w^2}X^2 + \left(-\frac{4}{w^2}x - \mathrm{i}k_d\cos\beta\right)X + \frac{2}{w^2}x^2\right)}$$
$$= \sqrt{\pi}\frac{w}{2} e^{-\frac{x^2}{w^2} + \frac{\mathrm{i}k_d x\cos\beta}{2} - \frac{k_d^2 w^2 \cos^2\beta}{16}}$$
$$\int \mathrm{d}Y e^{-\left(\frac{4}{w^2}Y^2 + \left(-\frac{4}{w^2}y - \mathrm{i}k_d\sin\beta\right)Y + \frac{2}{w^2}y^2\right)}$$
$$= \sqrt{\pi}\frac{w}{2} e^{-\frac{y^2}{w^2} + \frac{\mathrm{i}k_d y\sin\beta}{2} - \frac{k_d^2 w^2 \sin^2\beta}{16}} \tag{88}$$

From geometrical considerations (see Fig. 5) we find that

$$\begin{aligned} \mathrm{i}(\mathbf{k}_2 - \boldsymbol{\kappa})\cdot\boldsymbol{\rho} &= \mathrm{i}(k_2 \cos\alpha_2 - (\kappa_\perp \cos\theta_p - \kappa_\parallel \sin\theta_p))x \\ &\quad + \mathrm{i}(k_2 \sin\alpha_2 - (\kappa_\perp \sin\theta_p + \kappa_\parallel \cos\theta_p))y - \mathrm{i}\kappa_{\perp_z} z \end{aligned} \tag{89}$$

Since the measurement volume length L is much longer than the plasma minor radius a we find that

$$\int_{-L/2}^{L/2} \mathrm{d}z e^{-\mathrm{i}\kappa_{\perp_z} z} \approx \delta(\kappa_{\perp_z}) \tag{90}$$

Inserting Eqs. (89) and (90) into Eq. (87) and performing the integrations over x, y and z we arrive at

$$I_{12}(\mathbf{k}_1, \mathbf{k}_2, \omega) \propto \int \mathrm{d}Z \int \mathrm{d}\boldsymbol{\kappa} S(\boldsymbol{\kappa}, Z, \omega) e^{-\frac{k_d^2 w^2}{16}} e^{-\frac{w^2}{4}(c_1^2 + c_2^2)}$$
$$c_1 = \frac{k_d}{2}\cos\beta + k_2 \cos\alpha_2 - \kappa_\perp \cos\theta_p + \kappa_\parallel \sin\theta_p$$
$$c_2 = \frac{k_d}{2}\sin\beta + k_2 \sin\alpha_2 - \kappa_\perp \sin\theta_p - \kappa_\parallel \cos\theta_p, \tag{91}$$

where we have used that

$$\int_{-\infty}^{\infty} e^{-(ax^2 + bx)} \mathrm{d}x = \sqrt{\frac{\pi}{a}} e^{(b^2)/4a}$$
$$\int_{-\infty}^{\infty} e^{-\left(\frac{1}{w^2}x^2 - \mathrm{i}c_1 x\right)} \mathrm{d}x = \sqrt{\pi} w e^{-\frac{c_1^2 w^2}{4}}$$
$$\int_{-\infty}^{\infty} e^{-\left(\frac{1}{w^2}y^2 - \mathrm{i}c_2 y\right)} \mathrm{d}y = \sqrt{\pi} w e^{-\frac{c_2^2 w^2}{4}} \tag{92}$$

To perform the integration over $\boldsymbol{\kappa}$ we assume that $\kappa_\parallel \ll \kappa_\perp$

$$S(\boldsymbol{\kappa}, Z, \omega) = S(\boldsymbol{\kappa}_\perp, Z, \omega)\delta(\kappa_\parallel) \qquad \mathrm{d}\boldsymbol{\kappa} = \mathrm{d}\boldsymbol{\kappa}_\perp \mathrm{d}\kappa_\parallel, \tag{93}$$

so that

$$I_{12}(\mathbf{k}_1,\mathbf{k}_2,\omega) \propto \int \mathrm{d}Z S(\mathbf{k}_1,\mathbf{k}_2,Z,\omega) e^{-\frac{k_d^2 w^2}{16}} e^{-\frac{w^2}{4}(c_1^2+c_2^2)}$$

$$c_1 = \frac{k_d}{2}\cos\beta + k_2(\cos\alpha_2 - \cos\theta_p)$$

$$c_2 = \frac{k_d}{2}\sin\beta + k_2(\sin\alpha_2 - \sin\theta_p)$$

$$c_1^2 + c_2^2 = \frac{k_d^2}{4} + 2k_2^2(1-\cos(\alpha_2-\theta_p)) + k_2 k_d[\cos(\beta-\alpha_2) - \cos(\beta-\theta_p)] \quad (94)$$

We can reorganize the above equation to

$$I_{12}(\mathbf{k}_1,\mathbf{k}_2,\omega) \propto \int \mathrm{d}Z S(\mathbf{k}_1,\mathbf{k}_2,Z,\omega) \times e^{-\frac{w^2k_d^2}{2}(1-\cos(\alpha_2-\theta_p))} e^{-\frac{w^2}{4}\left(\frac{k_d^2}{2}+k_2k_d[\cos(\beta-\alpha_2)-\cos(\beta-\theta_p)]\right)} \quad (95)$$

The following relations exist

$$k_d = \sqrt{k_1^2 + k_2^2 - 2k_1k_2\cos(\alpha_2-\alpha_1)}$$

$$\beta = \arccos\left(\frac{k_1\cos\alpha_1 - k_2\cos\alpha_2}{k_d}\right), \quad (96)$$

meaning that Eq. (95) is fully determined by $\mathbf{k}_1, \mathbf{k}_2$ and ω.

d. Spatially separated measurement volumes. Eq. (76) means that turbulence in real space consists of elongated structures extended along the magnetic field lines. Since $\kappa_\perp$ is large, the structure size perpendicular to the magnetic field (i.e. cross-field) is modest. This in turn indicates that the cross-field correlation length $\mathcal{L}_\perp$ is small, experimentally found to be typically of order 1 cm [41]. The angle θ_R of the vector connecting the two measurement volumes is fixed, whereas θ_p varies with z. Letting **d** and **B** coincide at one volume, the difference between the two angles leads to the volumes being either connected or unconnected at the other volume, see Fig. 6. An approximate threshold criterion for the fluctuations in the volumes being correlated is

$$\sin(|\theta_R - \theta_p(z)|) = \frac{w+\mathcal{L}_\perp/2}{d}, \quad (97)$$

or

$$\theta_\perp(z) = |\theta_R - \theta_p(z)| \approx \frac{w+\mathcal{L}_\perp/2}{d} \quad (98)$$

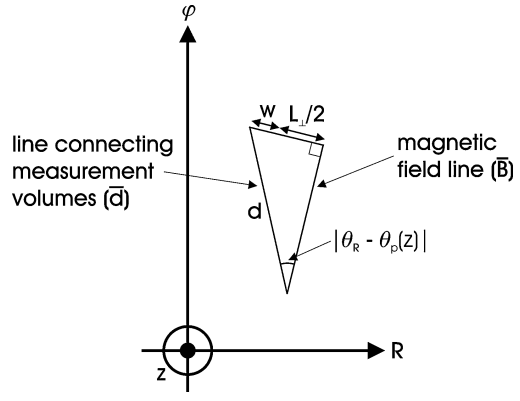

Fig. 6. Geometry concerning dual volume localization. Assuming that one of the measurement volumes is situated at the nadir of the triangle, **d** and **B** will diverge towards the second measurement volume. The threshold condition is shown (Eq. (97)), where the two volumes are borderline connected.

for small angles (in Ref. 2 we used $\theta_\perp(z) \approx \mathcal{L}_\perp/d$). This last formula allows us to distinguish between three cases:

1. $\theta_\perp(z) < \frac{w+\mathcal{L}_\perp/2}{d}$ for all z: The fluctuations in the volumes are correlated along the entire path.
2. $\frac{w+\mathcal{L}_\perp/2}{d} < \theta_\perp(z)$ for some z and $\theta_\perp(z) < \frac{w+\mathcal{L}_\perp/2}{d}$ for other z: The fluctuations are correlated for a section of the path.
3. $\theta_\perp(z) > \frac{w+\mathcal{L}_\perp/2}{d}$ for all z: The fluctuations in the volumes are uncorrelated along the entire path.

For experimental settings where case 2 is true, some localization can be obtained by calculating the crosspower spectrum between the volumes. In Ref. 4 we demonstrate this technique for a situation where $w = 4$ mm and $d = 29$ mm. This along with $\mathcal{L}_\perp = 1$ cm means that $\frac{w+\mathcal{L}_\perp/2}{d} \times \frac{180}{\pi} = 18^\circ$. The final issue is how to incorporate the measurement volume separation into the local spectral density $S(\mathbf{k}_1,\mathbf{k}_2,Z,\omega)$ from Eq. (95). Assuming that we work with frequency integrated measurements we can drop ω; further, we assume that S is independent of the wave vector. The remaining dependency is that of Z, the vertical coordinate along the measurement volumes. For the single volume case below, S is simply assumed to be proportional to δn^2, see Eq. (105). In the present case, however, we need to treat the correlation between the volumes. A plausible expression for the correlation function is

$$C_\perp(z) = \exp\left[-\left(\frac{|\theta_R - \theta_p(z)|d}{w+\mathcal{L}_\perp/2}\right)^2\right], \quad (99)$$

which is a Gaussian-type function. All quantities are known and independent of z except $\theta_p(z)$; but we should note that $\mathcal{L}_\perp$ could depend on z. The correlation function $C_\perp(z)$ possesses the expected limits:

- $C_\perp(z) = 1$ for $|\theta_R - \theta_p(z)| = 0$
- $C_\perp(z) = 1$ for $d = 0$
- $\lim_{w\to\infty} C_\perp(z) = 1$
- $\lim_{\mathcal{L}_\perp\to\infty} C_\perp(z) = 1$

For actual calculations we would replace S by $C_\perp(z) \times \delta n^2$ in Eq. (95) and use Eq. (107) for the density fluctuation profile. For the single volume simulations in the following we do not need to include $C_\perp(z)$.

One could argue that the pitch angle θ_p in the two spatially separated measurement volumes is different, so that the exponential functions in Eq. (95) would have to be modified. However, the actual distance between the volumes is small and therefore the pitch angles are almost identical.

2. Single volume

The material in this section is based on work presented in Ref. 42.

a. Single volume geometry. Fig. 7 shows the geometry associated with the single volume setup. The definitions are completely analogous to the ones in Fig. 3.

b. Localized autopower. The current spectral density (or autopower) for a single volume can be found from Eq. (95) by assuming that $k_d = 0$ and that we only have a single wave vector **k**

$$I_{11}(\mathbf{k},\omega) \propto \int \mathrm{d}Z S(\mathbf{k},Z,\omega) e^{-\frac{w^2k^2}{2}(1-\cos(\alpha-\theta_p))} \quad (100)$$

Assuming that the angles α and θ_p are small, we can expand the function in the exponent of Eq. (100) as

$$2k^2[1-\cos(\alpha-\theta_p)] \approx 2k^2[(\alpha-\theta_p)^2]/2 = k^2(\alpha-\theta_p)^2 \quad (101)$$

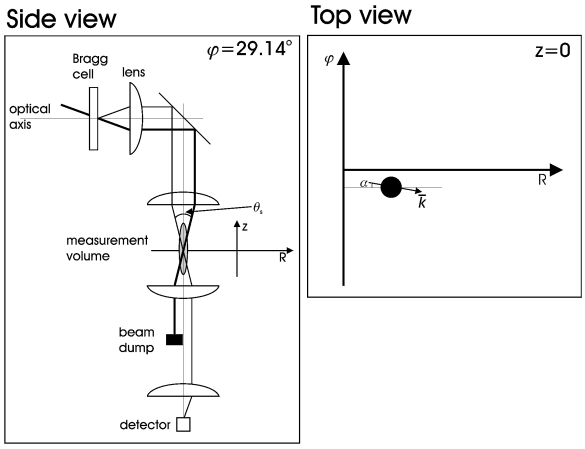

Fig. 7. Left: Schematic representation of the single volume setup (side view). Thick lines are the M beam, thin lines the LO beam, right: The single volume setup seen from above. The black dot is the measurement volume.

We introduce the instrumental selectivity function

$$\chi = e^{-\left(\frac{\alpha-\theta_p}{\Delta\alpha}\right)^2}, \tag{102}$$

where $\Delta\alpha = \frac{\Delta k}{k} = \frac{2}{kw}$ is the transverse relative wavenumber resolution. Using this instrumental function, the scattered power can be written

$$I_{11}(\mathbf{k},\omega) \propto \int \mathrm{d}Z S(\mathbf{k},Z,\omega) e^{-\left(\frac{\alpha-\theta_p}{\Delta\alpha}\right)^2} = \int \mathrm{d}Z S(\mathbf{k},Z,\omega)\chi \tag{103}$$

We will use this simplified equation to study how spatial resolution can be obtained indirectly. To make simulations for this purpose we need to assume a pitch angle profile and an expression for the frequency integrated local spectral density $S(\mathbf{k}, Z)$.

c. Modelled magnetic pitch angle. For our simulations we will take the pitch angle to be described by

$$\theta_p(r) = \arctan\left(\frac{B_\theta}{B_\varphi}\right) = \frac{r}{q_a R_0}(2 - 2\rho^2 + \rho^4)(2-\rho^2), \tag{104}$$

an analytical profile constructed by J. H. Misguich [42], see Fig. 8. Here, $\rho = r/a$ is the normalized minor radius coordinate, q_a is the magnetic field winding number at $r = a$ and R_0 is the major radius of the plasma. The total pitch angle variation $\Delta\theta_{p,\mathrm{tot}}$ is seen to be about 15°.

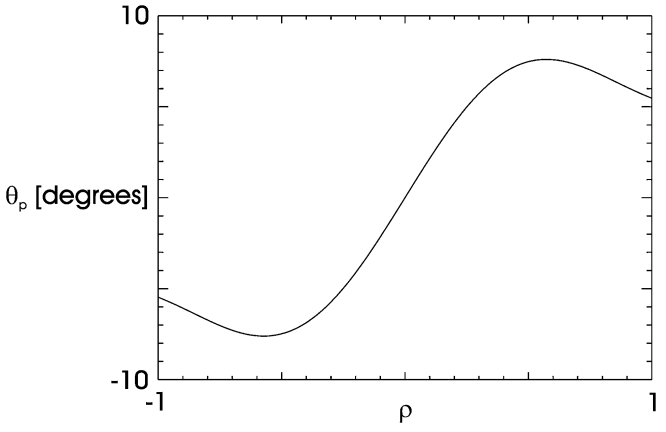

Fig. 8. Modelled pitch angle in degrees versus ρ. We have used $q_a = 3.3$, $R_0 = 2.38\,\mathrm{m}$ and $a = 0.75\,\mathrm{m}$ (Tore Supra parameters, see Ref. 42).

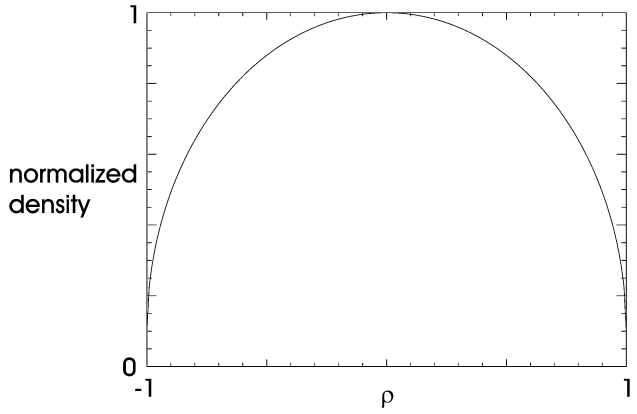

Fig. 9. Modelled normalized density versus ρ.

d. Fluctuation profiles. The frequency integrated local spectral density is assumed to be independent of the selected wave vector

$$S(\mathbf{k}, r) = S(r) = \delta n^2, \tag{105}$$

where we have replaced the beam coordinate Z by the radial coordinate r. The normalized density profile is assumed to be

$$\frac{n(r)}{n_0} = 0.1 + 0.9\sqrt{(1-\rho^2)}, \tag{106}$$

see Fig. 9.

Further, the relative density fluctuation profile is assumed to have the following structure

$$\frac{\delta n(r)}{n(r)} = b + c|\rho|^p, \tag{107}$$

where b, c and p are fit parameters. At present we will assume the following fit parameters: $b = 0.01$, $c = 0.1$ and $p = 3$, see the left-hand plot of Fig. 10.

e. Simulations. Above we have introduced spatially localized expressions for all external quantities entering Eq. (103). We set the wavenumber k to 15 cm^{-1} and the beam waist w to 2.7 cm. This means that the transverse relative wavenumber resolution $\Delta\alpha$ is equal to 2.8°. Fig. 11 shows χ for $\alpha = 0°$ (left) and 5° (right).

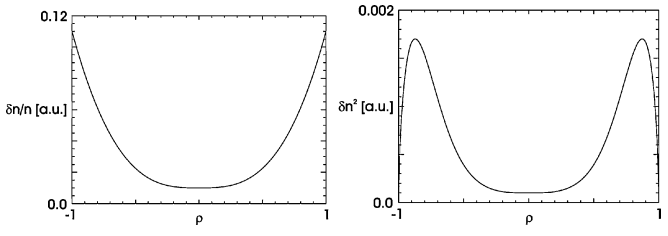

Fig. 10. Left: $\delta n/n$ versus ρ, right: δn^2 versus ρ.

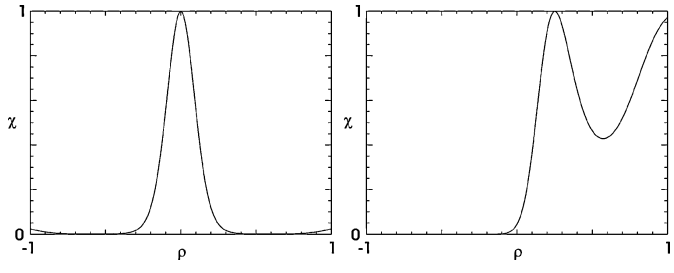

Fig. 11. Left: χ versus ρ for $\alpha = 0°$, right: χ versus ρ for $\alpha = 5°$ ($k = 15\,\mathrm{cm}^{-1}$, $w = 2.7\,\mathrm{cm}$).

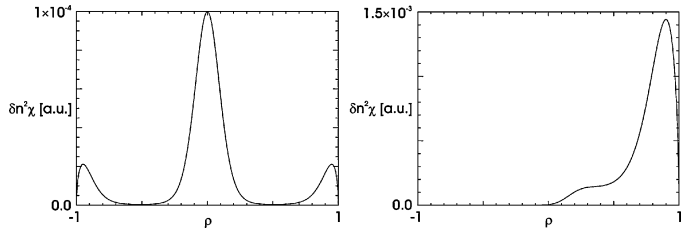

Fig. 12. Left: Integrand for $\alpha = 0^\circ$, right: Integrand for $\alpha = 5^\circ$ ($k = 15\,\mathrm{cm}^{-1}$, $w = 2.7\,\mathrm{cm}$).

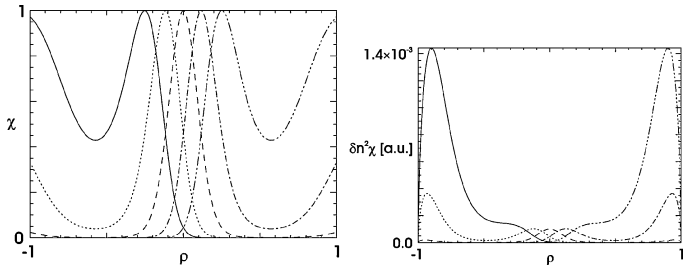

Fig. 13. Left: χ for five α values, right: Corresponding integrands ($k = 15\,\mathrm{cm}^{-1}$, $w = 2.7\,\mathrm{cm}$).

We observe that by changing the diagnostic angle α, χ changes position in the plasma.

Fig. 12 shows the integrand of Eq. (103) for the two cases shown in Fig. 11. We see that the 0° case corresponds to a signal originating in the central part of the plasma, while the 5° case detects edge fluctuations.

Fig. 13 shows figures corresponding to Figs. 11 and 12, but now for a mini α-scan: $[-5^\circ, -2.5^\circ, 0^\circ, 2.5^\circ, 5^\circ]$.

Fig. 14 shows the integrands in Fig. 13 integrated along $\rho\,(= I_{11})$.

Finally, Fig. 15 shows the effect of increasing the transverse relative wavenumber resolution $\Delta\alpha$ from 2.8° to 28.0°. The instrumental selectivity function (left) becomes extremely broad, leading to the total scattered power having no significant variation with α.

What we have demonstrated with the above simulations is that for localization to be possible, the following has to be true

$$\Delta\theta_{p,\mathrm{tot}}[\mathrm{degrees}] \gg \Delta\alpha[\mathrm{degrees}] = \frac{2}{kw} \times \frac{180}{\pi} \tag{108}$$

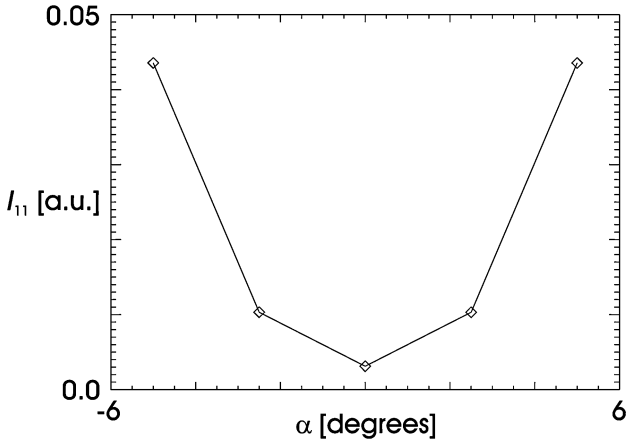

Fig. 14. Total scattered power (I_{11}) versus α ($k = 15\,\mathrm{cm}^{-1}$, $w = 2.7\,\mathrm{cm}$).

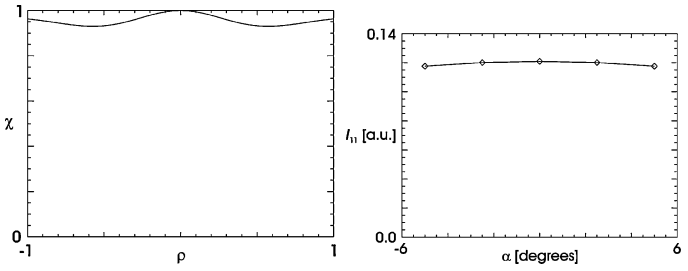

Fig. 15. Left: χ for $\alpha = 0$ degrees versus ρ, right: Total scattered power (I_{11}) versus α ($k = 15\,\mathrm{cm}^{-1}$, $w = 0.27\,\mathrm{cm}$).

For examples where this technique was used to measure turbulence profiles see Refs. 5, 42, 43.

3. Discussion

We end the section with a brief discussion on the dual and single volume localization criteria. The single volume criterion has already been written in Eq. (108). To discuss the dual volume criterion in more detail, we introduce $\Delta\theta_{\perp,\mathrm{tot}}$, which is the maximum absolute difference between θ_R and $\theta_p(z)$ assuming that they are equal at some z (case 2 in section III C 1). The dual volume localization condition for this situation is

$$\Delta\theta_{p,\mathrm{tot}}[\mathrm{degrees}] \geq \Delta\theta_{\perp,\mathrm{tot}}[\mathrm{degrees}] \gg \frac{w + \mathcal{L}_\perp/2}{d} \times \frac{180}{\pi} \tag{109}$$

Alternatively, even if this criterion is not fulfilled (case 1), some localization can be obtained using case 3: If θ_R is set so that it is outside the plasma (does not coincide with $\theta_p(z)$ for any z), measurements weighted towards the top and bottom of the plasma can be made [4].

IV. Conclusions

In section II, we derived an expression for the detected photocurrent from first principles. Thereafter demodulation was explained, phase separation of the detected signal was interpreted and an expression for the density fluctuations squared was presented. Finally, a simple example illustrated this density fluctuation formula for Gaussian beams.

In section III, the measurement volume was treated in detail. The simple geometrical estimate was compared to a more elaborate treatment. Following this, direct and indirect localization was discussed, and general expressions for auto- and crosspower were derived. A discussion ensued, and finally simulations assisted in the interpretation of localized autopower from a single measurement volume.

Acknowledgments

N.P.B. wishes to thank J.-H. Chatenet and G. Y. Antar for providing reports and Ph.D. theses treating the ALTAIR collective scattering diagnostic, H. Smith for his careful reading of and suggestions concerning section II and M. Saffman for guidance during the initial stages of this work.

N.P.B. was supported at MIT by the U.S. Department of Energy, Cooperative Grant No. DE-FC02-99ER54512.

References

1. Renner, H. *et al.*, "Initial Operation of the Wendelstein 7AS advanced stellarator," Plasma Phys. Control. Fusion **31**, 1579–1596 (1989).
2. Saffman, M., Zoletnik, S., Basse, N. P. *et al.*, "CO_2 laser based two-volume collective scattering instrument for spatially localized measurements," Rev. Sci. Instrum. **72**, 2579–2592 (2001).

3. Basse, N. P., Zoletnik, S., Saffman, M. *et al*., "Low- and high-mode separation of short wavelength turbulence in dithering Wendelstein 7-AS plasmas," Phys. Plasmas **9**, 3035–3049 (2002).
4. Zoletnik, S., Basse, N. P., Saffman, M. *et al*., "Changes in density fluctuations associated with confinement transitions close to a rational edge rotational transform in the W7-AS stellarator," Plasma Phys. Control. Fusion **44**, 1581–1607 (2002).
5. Basse, N. P., Michelsen, P. K., Zoletnik, S. *et al*., "Spatial distribution of turbulence in the Wendelstein 7-AS stellarator," Plasma Sources Sci. Technol. **11**, A138–A142 (2002).
6. Basse, N. P., Turbulence in Wendelstein 7-AS plasmas measured by collective light scattering, Ph.D. thesis (2002), http://www.risoe. dk/rispubl/ofd/ris-r-1355.htm.
7. Basse, N. P., Zoletnik, S., Bäumel, S. *et al*., "Turbulence at the transition to the high density H-mode in Wendelstein 7-AS plasmas," Nucl. Fusion **43**, 40–48 (2003).
8. Basse, N. P., Zoletnik, S., Antar, G. Y. *et al*., "Characterization of turbulence in L- and ELM-free H-mode Wendelstein 7-AS plasmas," Plasma Phys. Control. Fusion **45**, 439–453 (2003).
9. Mazzucato, E., "Localized measurement of turbulent fluctuations in tokamaks with coherent scattering of electromagnetic waves," Phys. Plasmas **10**, 753–759 (2003).
10. Maiman, T. H., "Stimulated optical radiation in Ruby," Nature **187**, 493 (1960).
11. Surko, C. M. and Slusher, R. E., "Study of the density fluctuations in the Adiabatic Toroidal Compressor scattering tokamak using CO_2 laser," Phys. Rev. Lett. **37**, 1747–1750 (1976).
12. Slusher, R. E. and Surko, C. M., "Study of density fluctuations in plasmas by small-angle CO_2 laser scattering," Phys. Fluids **23**, 472–490 (1980).
13. Watterson, R. L., Slusher, R. E. and Surko, C. M., "Low-frequency density fluctuations in a tokamak plasma," Phys. Fluids **28**, 2857–2867 (1985).
14. Truc, A. *et al*., "Correlation between low frequency turbulence and energy confinement in TFR," Nucl. Fusion **26**, 1303–1310 (1986).
15. Boileau, A. and Lachambre, J.-L., "Density fluctuations dispersion measurement in the Tokamak de Varennes," Phys. Lett. A **148**, 341–344 (1990).
16. Truc, A. *et al*., "ALTAIR: An infrared laser scattering diagnostic on the Tore Supra tokamak," Rev. Sci. Instrum. **63**, 3716–3724 (1992).
17. Bulanin, V. V., Vers, A. V., Esipov, L. A. *et al*., "A study of low-frequency microturbulence by CO_2-laser collective scattering in the FT-2 tokamak," Plasma Phys. Rep. **27**, 221–227 (2001).
18. Brower, D. L., Peebles, W. A. and Luhmann, Jr. N. C., "The spectrum, spatial distribution and scaling of microturbulence in the TEXT tokamak," Nucl. Fusion **27**, 2055–2073 (1987).
19. Holzhauer, E. and Dodel, G., "Collective laser light scattering from electron density fluctuations in fusion research plasmas," Rev. Sci. Instrum. **61**, 2817–2822 (1990).
20. Philipona, R., Doyle, E. J., Luhmann, Jr. N. C. *et al*., "Far-infrared heterodyne scattering to study density fluctuations on the DIII-D tokamak," Rev. Sci. Instrum. **61**, 3007–3009 (1990).
21. Coda, S., Porkolab, M. and Carlstrom, T. N., "A phase contrast interferometer on DIII-D," Rev. Sci. Instrum. **63**, 4974–4976 (1992).
22. Kado, S., Nakatake, H., Muraoka, K. *et al*., "Density fluctuations in Heliotron E measured using CO_2 laser phase contrast method," Fusion Eng. and Design **34–35**, 415–419 (1997).
23. Mazurenko, A., Porkolab, M., Mossessian, D. *et al*., "Experimental and theoretical study of quasicoherent fluctuations in enhanced D_α plasmas in the Alcator C-Mod tokamak," Phys. Rev. Lett. **89**, 225004 (2002).
24. Surko, C. M. and Slusher, R. E., "Study of plasma density fluctuations by the correlation of crossed CO_2 laser beams," Phys. Fluids **23**, 2425–2439 (1980).
25. Hutchinson, I. H., Principles of plasma diagnostics, (Cambridge University Press, Cambridge, 2002), 2nd ed.
26. Salpeter, E. E., "Electron density fluctuations in a plasma," Phys. Rev. **120**, 1528–1535 (1960).
27. Elbek, B., Elektromagnetisme, (Niels Bohr Institutet, Copenhagen, 1994).
28. Kleppner, D. and Kolenkow, R. J., An introduction to mechanics, (McGraw-Hill, New York, 1978).
29. Grésillon, D., Stern, C., Hémon, A. *et al*., "Density fluctuation measurement by far infrared light scattering," Physica Scripta **T2/2**, 459–466 (1982).
30. Saffman, M., Operating procedures, CO_2 laser collective scattering diagnostic at W7-AS, Notes (2000).
31. Honoré, C., Le signal complexe de la diffusion collective de la lumière et les écoulements turbulents, Ph.D. thesis (1996).
32. Jackson, J. D., Classical electrodynamics, (John Wiley and Sons, New York, 1962).
33. Born, M. and Wolf, E., Principles of optics, (Cambridge University Press, Cambridge, 1999).
34. Holzhauer, E. and Massig, J. H., "An analysis of optical mixing in plasma scattering experiments," Plasma Physics **20**, 867–877 (1978).
35. Spiegel, M. R., Mathematical handbook, (McGraw-Hill, New York, 1991).
36. Antar, G., Observation des petites échelles de la turbulence développée par diffusion collective de la lumière, Ph.D. thesis (1996).
37. Menicot, O., Etude des fluctuations de densité dans les plasmas de tokamak: Application à l'interspectre du signal turbulent, PMI report 2972 (1994).
38. Heinemeier, N. P., Flow speed measurement using two-point collective light scattering, M.Sc. thesis (1998), http://www.risoe.dk/rispubl/ofd/riso-r-1064.htm.
39. Antar, G., Devynck, P., Laviron, C. *et al*., "Temporal separation of the density fluctuation signal measured by light scattering," Plasma Phys. Control. Fusion **41**, 733–746 (1999).
40. Antar, G., Gervais, F., Hennequin, P. *et al*., "Statistical study of density fluctuations in the Tore Supra tokamak," Plasma Phys. Control. Fusion **40**, 947–966 (1998).
41. Zoletnik, S., Anton, M., Endler, M. *et al*., "Density fluctuation phenomena in the scrape-off layer and edge plasma of the Wendelstein 7-AS stellarator," Phys. Plasmas **6**, 4239–4247 (1999).
42. Devynck, P., Garbet, X., Laviron, C. *et al*., "Localized measurements of turbulence in the Tore Supra tokamak," Plasma Phys. Control. Fusion **35**, 63–75 (1993).
43. Antar, G., Hoang, G. T., Devynck, P. *et al*., "Turbulence reduction and poloidal shear steepening in reversed shear plasmas investigated by light scattering on Tore Supra," Phys. Plasmas **8**, 186–192 (2001).